

Received October 26, 2020; reviewed; accepted January 16, 2021

Experimental research on the strength distribution of brittle spheres under compression

Qiang Zhou ¹, Qing Guo ¹, Yongtai Pan ¹, Changyong Zhu ², Yinghua Wei ²

¹ China University of Mining and Technology Beijing, School of Chemical and Environmental Engineering, Beijing, 100083, China

² Shenhua Ningxia Coal Industry Group CO., LTD Taixi CPP, Ningxia Shi Zuishan 753000, China

Corresponding author: pan_yongtai@126.com (Yongtai Pan)

Abstract: The strength of a particle is one of the most crucial characteristics within a comminution process due to the mechanical stresses experienced by each particle. In this study, the K9 glass spheres and ceramic spheres were subjected to a breakage test. The test includes the breakage of up to 240 particles under compression to obtain the distribution of the breakage probability depending on the crushing force and breakage energy. The breakage test was conducted for five particle size fractions from each individual material. Thus obtained 10 crushing force distributions and corresponding 10 breakage energy distributions were fitted with lognormal distribution function. The parameters in the lognormal were analyzed including the effect of the material and particle size. Following this, the relationship between the crushing force and breakage energy was analyzed based on the Hertzian elastic contacts model and Tomas's elastic-plastic contact model, respectively. Additionally, particle strength in terms of crushing force and breakage energy were compared and found to be size dependent. Finally, a simple transformation algorithm of distributions is developed. According to this algorithm the crushing force distribution can be transformed into breakage energy distribution and vice versa. The findings facilitate a better understanding of the particle strength distribution under compression and will help to improve the comminution process design, control and optimization.

Keywords: particle strength, breakage energy, crushing force, lognormal function, breakage probability

1. Introduction

Particle breakage represents the most elementary process in comminution (Wu et al., 2004). Numerous studies have been dedicated to the efficiency of the process of comminution and breakage model (Nadolski et al., 2014; Martins, 2016; Shi, 2016; Shi and Kojovic, 2007; Tromans, 2008; Fuerstenau et al., 2002; Vogel and Peukert, 2003). Fragmentation of a single particle is commonly used to better understand the fragmentation process, particularly in terms of energy utilization by comminution and the establishment of breakage function and selection function to predict particle size distribution.

Many studies have been focused on the phenomenon of particle fragmentation. In general, several different types of compressive loading have been used in experimental studies: slow compression testing machines, drop weight testing, pendulum testing, single particle impact testing, Hopkinson pressure bar, impact load cell, and ballistic loading (Zhang, 2014). Investigations using these methods were performed over a restricted range of stress rate because particle characteristics depend on stress rate. The stress rate that is applied by common comminution technologies varies from 10^{-3} to 10^2 s⁻¹. In such cases, the effect of stress rate on wave propagation is negligible, and hence it is very unlikely that the change in stress rate in slow compression test or in drop weight impact test will have a significant influence on particle breakage. Therefore, the slow compression test is proposed to be carried out widely (Tavares and King, 1998; Liburkin et al., 2015). Slow compression tests on spheres have been applied to different materials, such as glass and soda-lime glass (Chau et al., 2000; Chaudhri, 2004; Huang et al.,

2014). The compression of spheres between two flat platens has been proposed for testing the deformability of elastic materials, hardness of ductile materials and crushing strength of brittle materials (Portnikov and Kalman, 2014). Nadolski (2014), Aman (2010), and Rozenblat (2011) used irregular particles under slow compression to obtain particle breakage energy, breakage probability distribution, particle strength, particle stiffness, specific energy-progeny size distribution, and energy utilization.

Since particles, even of the same material and equal size, are not identical, the strength has to be described by a statistical distribution (Gundepudi, 1997). In the majority of cases the particle strength distribution (PSD) was described by the Weibull distribution (Couroyer et al., 2003; Wong et al., 2005; Huang et al., 2014; Sun et al., 2020). However, some researchers used the lognormal distribution to express strength distribution (Aman, 2009; Tavares and Almeida, 2020). Additionally, particle strength is usually expressed by stress terms, i.e. there are cases where strength is expressed in breakage energy, crushing force and specific energy terms (Rozenblat et al., 2011). Crushing force and breakage energy are essential parameters in designing comminution geometry and in predicting the power and the comminution energy efficiency (Aman et al., 2010; Rozenblat et al., 2011). Crushing force can be obtained directly and accurately by the slow compression test. However, the breakage energy can be calculated as an integral of the compression force with respect to the displacement. There are no difficulties that exist in force measurement, but the measurement of deformations requires taking into account the contact deformation of the tools, particularly for small hard particles. Tavares (1998) and Sun (2020) studied that the stiffness of the tool influences the particle breakage energy and energy efficiency. The inaccuracy in the determination of particle deformation leads to additional errors in the breakage energy.

Even though different types of testing methods have been used for single particle tests proven by abundance of reference data in the current literature, only limited attention has been given to the relationship between crushing force and breakage energy. In this study, the PSD was based on the lognormal function of crushing force and breakage energy of a number of individual particles. The parameters in the lognormal function were investigated and their dependency on the mechanical properties of the particulate materials was found. The relationship between the crushing force and breakage energy of the brittle sphere under compression was established and analyzed.

2. Theoretical approaches

2.1. Hertzian elastic contact model (Johnson,1985)

Whenever bodies of curved surfaces are in contact, a relative indentation in the vicinity of the contact point in addition to the gross or bulk deformation of the objects as a whole will take place. Hertz developed a theory that describes the stresses and deformations near the contact point of colliding bodies as a function of their geometric and elastic properties. Some of the assumptions in Hertzian contact theory are: (1) contact is perfectly lubricated and no friction exists; (2) bodies behave perfectly elastically; (3) contact is perfectly elastic; (4) contact area is small compared to the dimensions of the contacting bodies; (5) deformations are small. Considering the above some assumptions, the relationship between contact force (F) and deformation (s) is given by:

$$F = \frac{4}{3}E^*\sqrt{R^*}s^{3/2} \quad (1)$$

$$E^* = \left(\frac{1-\nu_1^2}{E_1} + \frac{1-\nu_2^2}{E_2}\right)^{-1}, \quad R^* = \left(\frac{1}{R_1} + \frac{1}{R_2}\right)^{-1}$$

where R^* and E^* are the effective diameter and the effective modulus of elasticity of the spherical body, ν_i , E_i and R_i ($i = 1,2$) respectively represent Poisson's ratio of the material, the Young's modulus and radius of geometry. The number 1 and 2 stands for sphere and loading geometry.

At the breakage point $s = s_B$ the breakage force F_B can be obtained:

$$F_B = \frac{4}{3}E^*\sqrt{R^*}s_B^{3/2} \quad (2)$$

The breakage energy during a test in the slow compression can be calculated directly using Eq. (1) from numerical integration of the contact force-deformation profile.

$$W_B = \int_0^{s_B} F ds = \int_0^{s_B} \frac{4}{3} E^* \sqrt{R^*} U^{3/2} ds = \frac{8}{15} E^* \sqrt{R^*} s_B^{5/2} \quad (3)$$

As a result, the ratio F_B / W_B is given by:

$$\frac{F_B}{W_B} = \frac{2.5}{s_B} \quad (4)$$

2.2. Tomas's elastic-plastic contact model (Tomas, 2000; Antonyuk et al., 2010)

The repulsive force by the elastic-plastic contact deformation without any adhesion is proportional to the particle size d and micro-yield strength p_F :

$$F = \pi \frac{ds}{2} p_F \left[1 - \frac{1}{3} \sqrt[3]{\frac{s_F}{s}} \right] \quad (5)$$

where s_F is the contact displacement at the yield point of the spheres.

$$s_F = \frac{d}{2} \left(\frac{\pi p_F}{E^*} \right)^2 \quad (6)$$

The yield point s_F corresponds to the maximum elastic pressure within the contact circle that leads to the elastic-plastic deformation of the sphere. At the breakage point $s=s_B$ the crushing force F_B can be obtained:

$$F_B = \pi \frac{ds_B}{2} p_F \left[1 - \frac{1}{3} \sqrt[3]{\frac{s_F}{s_B}} \right] \quad (7)$$

Breakage energy W_B is defined as the energy stored by the particle until the instant of fracture and it corresponds to the area below the force-deformation curve, which is calculated as follows:

$$W_B = \int_0^{s_B} F(s) ds = \int_0^{s_B} \pi \frac{d}{2} p_F \left[s - \frac{s^{2/3} s_F^{1/3}}{3} \right] ds = \pi \frac{d}{2} p_F s_B^2 \left[\frac{1}{2} - \frac{1}{5} \sqrt[3]{\frac{s_F}{s_B}} \right] \quad (8)$$

As a result, the ratio F_B / W_B is given by:

$$\frac{F_B}{W_B} = \frac{1}{s_B f \left(\frac{s_F}{s_B} \right)} \quad (9)$$

where $f \left(\frac{s_F}{s_B} \right) = \left(\frac{1}{2} - \frac{1}{5} \sqrt[3]{\frac{s_F}{s_B}} \right) / \left(1 - \frac{1}{3} \sqrt[3]{\frac{s_F}{s_B}} \right)$.

The function f varies about 8.4% with increasing ratio s_B/s_F from 1 to 30, (see Fig. 1). Consequently, the ratio s_B/s_F changes only a little with the particle size. Thus, the function f can be considered as a size independent function.

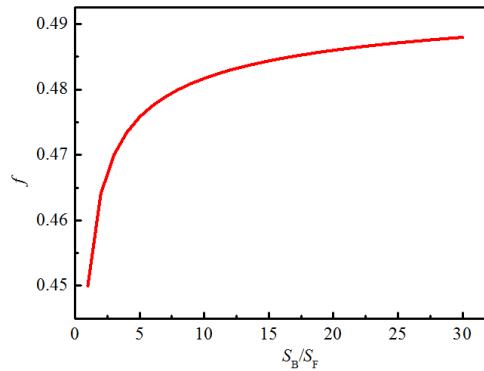


Fig. 1. The variation of function f with s_B/s_F

3. Materials and methods

3.1. Materials

The K9 glass spheres and ceramic spheres are used as the experimental material. The spherical morphology eliminates the complications caused by the irregular shapes of real particles. The chemical composition of the K9 glass and ceramic samples using X-ray fluorescence (XRF) spectrometry in Table 1 shows that they are mainly composed of silicon dioxide (69.13% and 74.96%) for the K9 glass and ceramic spheres, respectively.

Mass of the spheres was obtained using an electronic balance (accuracy: ± 0.01 g), and the diameters of the three vertical directions of the spheres were measured using a Vernier calliper (accuracy: ± 0.02 mm). The density of K9 glass sphere and ceramic sphere are 2540 kg/m^3 and 2400 kg/m^3 , respectively. The means and standard deviations of the sphere diameters and mass calculated from more than 240 samples are listed in Table 2.

The standard deviations of the diameter and mass of the K9 glass spheres and ceramic spheres (shown in Table 2) are much smaller than their means, indicating that the spheres are of good uniformity in size. The samples of K9 glass spheres and ceramic spheres are presented Fig. 2.

Table 1. Chemical composition of the K9 glass and ceramic samples

Material	Measure	Value (%)
K9 glass sphere	SiO ₂	69.13
	B ₂ O ₃	10.75
	K ₂ O	6.29
	Na ₂ O	10.40
	As ₂ O ₃	0.36
	BaO	3.07
Ceramic sphere	SiO ₂	74.96
	Al ₂ O ₃	18.50
	Fe ₂ O ₃	1.39
	TiO ₂	0.35
	CaO	0.16
	MgO	0.28
	K ₂ O	3.50
	Na ₂ O	0.27

Table 2. Basic physical characteristics of K9 glass sphere and ceramic sphere

Material	Diameter (mm)	Mass (g)
K9 glass sphere	9.90 ± 0.10	1.31 ± 0.22
	19.14 ± 0.16	9.32 ± 0.32
	29.64 ± 0.23	34.64 ± 0.42
	39.22 ± 0.27	79.28 ± 0.47
	48.76 ± 0.32	151.19 ± 0.52
Ceramic sphere	10.00 ± 0.23	1.26 ± 0.20
	19.18 ± 0.21	8.88 ± 0.32
	30.42 ± 0.28	35.40 ± 0.36
	37.88 ± 0.31	68.33 ± 0.37
	51.49 ± 0.41	171.49 ± 0.42

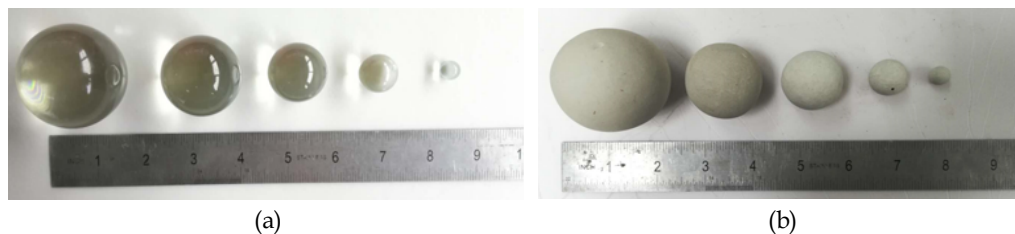


Fig. 2. Experimental materials: (a) the K9 glass spheres with five diameters; (b) ceramic spheres with five diameters

3.2. Apparatus and experimental methods

The experimental setups are presented in Fig. 3. Fig. 3b shows the compression setups, i.e., the material test system (TAW-3000) and the high-speed photography system. The TAW-3000 hydraulic servo test

system was equipped with a load cell with a measuring capacity of 3000 kN and a resolution of 20 N. All the compression tests were performed with the TAW-3000 at a constant loading rate of 0.2 mm/min, which is low enough to make the inertial effects negligible. The high-speed camera was used to capture the catastrophic breakage process of the spheres. However, the performance of high-speed camera (a maximum of 2000 frames to be captured per second) failed to record the growth of the crack. Therefore, the results will not be discussed in the present work. This has little influence on the following discussions which mainly focus on the particle strength of the spheres. A transparent plastic wall was used to gather the fragmentation debris of the spheres and protect the operator and the camera in case of debris splash. The enlarged graph of the loading cell is shown in Fig. 3 (a). The tested material was sandwiched between the blocks with a thin layer of petrolatum in between to reduce friction. Upon loading, the lower platen compressed the sphere from the bottom up at a loading rate of 0.2 mm/min while the upper platen was fixed. The loading stopped when the sphere underwent a catastrophic failure and the axial stress exhibited a sharp decrease from the maximum load. The axial force was measured by the force sensor embedded in the upper platen. The axial displacement, i.e., the displacement of the lower platen, was measured by the displacement sensor embedded in the lower platen.

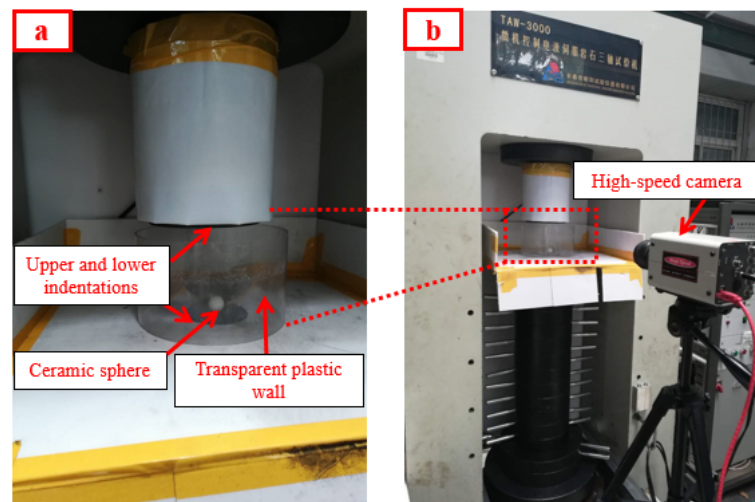


Fig. 3. TAW-3000 hydraulic servo test system

4. Results and discussion

4.1. The typical compression force-displacement curve of K9 glass spheres and ceramic spheres

For each kind of spheres about 24 samples are tested to provide sufficient data for the subsequent statistical analyses of the breakage strengths of glass and ceramic materials. More than 240 K9 glass and ceramic spheres of five different sizes were subjected to uniaxial compression experiments and obtained 240 compressive force-displacement curves. The typical compression curve of the spheres with $\Phi 19.12$ mm is presented in Fig. 4. The force-displacement curve can be divided into two stages including elastic deformation and plastic deformation. The elastic deformation stage is consistent with the theoretical Hertz curve. The yield point where the force-displacement curve deviates from the Hertz curve corresponds to the last 0.08 mm of deformation before fracture. At the failure point, the sphere undergoes a catastrophic failure and the axial force exhibits a sharp decrease to zero. Therefore, the deformation of the glass sphere is dominantly elastic-brittle and the slight plasticity mainly concentrates around the contact area (Sun et al., 2019). It can be found that $s_B/s_F \approx 0.85$, and the function f is about 0.45. Since the coefficient of determination was 0.996, the Hertzian model can be used to calculate the crushing force, breakage energy and the ratio F_B / W_B .

4.2 Initial particle strength distribution

Particle strength is defined as the ability to withstand an applied force and energy input up to a certain limit of failure or breakage. Due to the presence of pores, defects such as micro cracks and impurities,

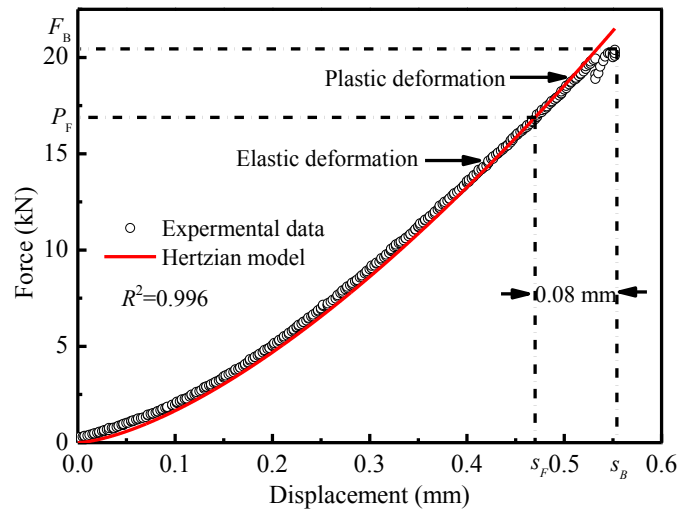


Fig. 4. Typical force-displacement curve

the strength of particles is not uniform and therefore must be described by a statistical distribution. There are many statistical distribution models that describe PSD such as the Gauss distribution (Couroyer et al., 2003), logistic function (Rozenblat et al., 2011, Sun et al., 2020), Weibull function (Huang et al., 2014), and lognormal function (Tavares and Almeida, 2020). In this paper the lognormal function will be used to fit the PSD.

The PSD can be presented in terms of: crushing force – the force at which the particle breaks; breakage energy – energy that was applied in order to break the particle; fracture stress – the stress required to break the particle; and the specific energy – breakage energy per particle volume or mass. In this paper in terms of the crushing force and breakage energy are used to describe the particle strength.

The crushing force is measured at the point at which there is a sudden large increase of the displacement with an associated decrease in force. The F_B represents the crushing force in Fig. 4. The breakage energy is the integration of the crushing force with respect to displacement of the particle, as demonstrated in Eq. (3).

Whenever the crushing force and breakage energy of K9 glass spheres and ceramic spheres in a sample of a given size were measured, a large scatter of the experimental data appeared. Such variability must be described in details by using order statistics. Order statistics is a statistical method which is commonly used to deal with variable data. The breakage probability P of the particles can be calculated with the probability estimators. It consists of ranking the test results in ascending order and then assigning $i = 1, 2, \dots, N$ to the ranked experimental data, where N is the total number of valid tests. The cumulative distributions for the crushing force and breakage energy of the tested particles are estimated by:

$$P = \frac{i-0.5}{N} \quad (9)$$

The data from the tests can be fitted to empirical cumulative distribution functions and their characteristic parameters can be estimated. The lognormal distribution has been selected, and is given by:

$$P(F_B) = \frac{1}{2} \left[1 + \operatorname{erf} \left(\frac{\ln F_B - \ln F_{B,50}}{\sqrt{2\sigma_F^2}} \right) \right] \quad (10)$$

where P is the breakage probability of the particle, $F_{B,50}$ and σ_F^2 are the median value and variance of the distribution respectively. Note that Eq. (10) could be rewritten for expressing the probability distribution of the breakage energy by replacing F_B with W_B in the equation.

The experimental data points and the corresponding fitting curves according to Eq. (10) for the K9 glass spheres and ceramic spheres with five different sizes are shown in Fig. 5. As can be seen in

Figs. 5 (a), (b), (d) and (e), in order to achieve the same breakage probability, large particles require higher crushing force and breakage energy, since crushing force and breakage energy is directly dependednt on the particle size (Rozenblat et al., 2011). However, as it is seen in Figs. 5 (c) and (f), smaller particles are stronger than larger particles. Shi (2007) found that the crack density of large particles is much greater than that for smaller particles. In view of this, bigger particles tend to be weaker and therefore easier to break than smaller particles. The quantitative basis of comparison of the lognormal model to the experimental data is usually presented by the coefficients of determination (R^2). The R^2 and empirical parameters of the strength distribution in terms of crushing force and breakage energy are presented in Table 3.

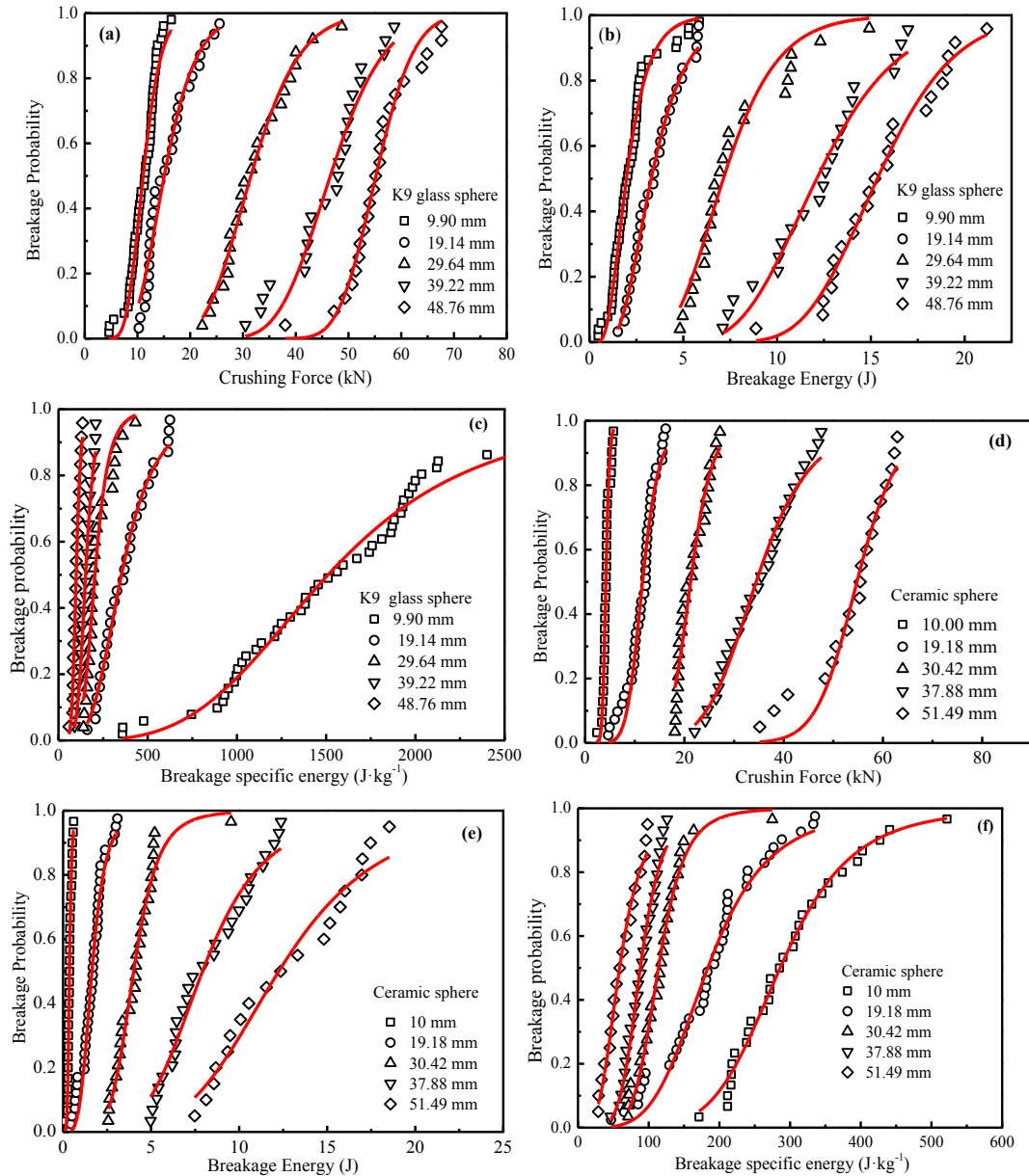


Fig. 5. Lognormal function fitting to the experimental data of various materials and sizes

4.3. The relationship between the median and variance of the strength distribution and particle size

Figs. 6 (a) and (b) demonstrates the linear dependency of the median breakage energy and the median crushing force on the square of the particle size for K9 glass spheres and ceramic spheres. The same effect was reported by Rumpf (1973) and Hiramatsu (1966). The variances of distribution were investi-

Table 3. Fitting summary for the K9 glass spheres and ceramic spheres

Material	Size interval/mm	Crushing force			Breakage energy		
		$F_{B,50}$ /kN	σ_F	R^2	$W_{B,50}$ /J	σ_W	R^2
K9 glass sphere	9.90	11.02	0.34	0.978	1.97	0.47	0.987
	19.14	15.03	0.31	0.967	3.29	0.44	0.992
	29.64	31.50	0.23	0.987	7.17	0.31	0.956
	39.22	46.53	0.17	0.958	12.06	0.28	0.973
	48.76	55.15	0.10	0.980	15.33	0.21	0.982
\bar{R}^2				0.974			0.978
Ceramic sphere	10.00	4.18	0.15	0.970	0.36	0.31	0.982
	19.18	11.59	0.24	0.971	1.64	0.39	0.972
	30.42	21.33	0.18	0.956	4.01	0.29	0.974
	37.88	34.47	0.26	0.988	7.92	0.36	0.978
	51.49	54.60	0.13	0.959	12.18	0.38	0.968
\bar{R}^2				0.969			0.975

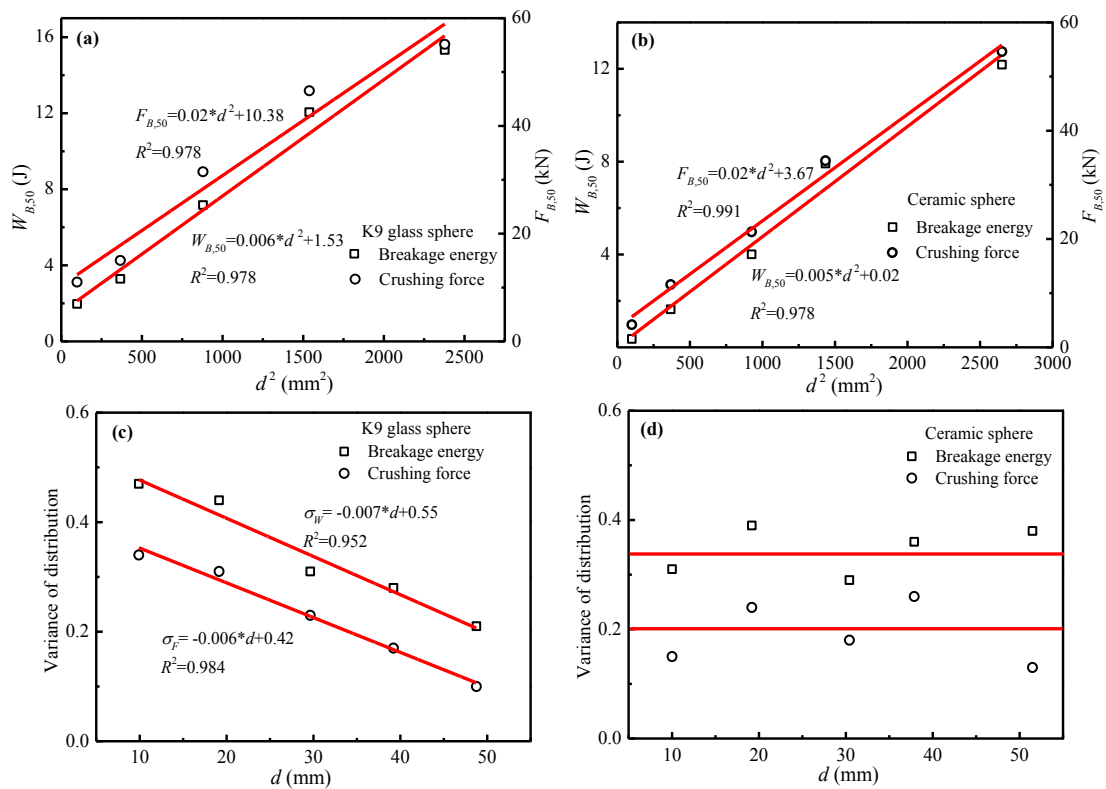


Fig. 6. Relationship between the median and variance of strength distribution and particle size

gated and found to be linearly decreased with the increase of particle diameter for the K9 glass spheres, as presented Fig. 6(c). However, for the ceramic sphere variance of distribution was found to be a weak function of particle size and therefore assumed to be a function of the material only and independent of particle size (as shown Fig. 6 (d)). It could be explained by the result of the microstructure of the material and the number of tests (Huang et al., 2014). For example, the microstructure of the particles, including the nanopores within, as well as the size, direction, shape, and distribution of the cracks have great impacts on the crushing force and breakage energy. The second reason is that the standard deviation of the particle strength cannot be accurately measured with about 25 tests. Therefore, increasing the number of tests may reduce the variability of the variance of the distribution for ceramic spheres. The relationship between the variance of the distribution and size will be addressed in future investigations.

4.4. The relationship between the crushing force and breakage energy

As mentioned above, the relationship between crushing force and breakage energy was analyzed based on theoretical approaches. It was found that the ratio of crushing force and breakage energy depends on s_B or s_B/s_F . In section 4.1, it was found that $s_B/s_F \approx 0.85$ for the brittle material. The function f varies by about 8.4% with the ratio s_B/s_F increased from 1 to 30, shown in Fig. 1. Thus, the function f can be considered as a size-independent function. Therefore, it is interesting to investigate the relationship between s_B and particle sizes.

As shown in Fig. 7 breakage point s_B was found to be linearly dependent on the diameter of particles for the K9 glass spheres and the ceramic spheres at a specific size range. Alternatively, some scholars found that breakage point s_B was a weak function of particle size, which was assumed to be a function of the material only and independent of particle size at the narrow size range (Aman et al., 2010). This hypothesis was only applicable to certain situations with a narrow size range. In section 4.2, Fig. 5, and Table 3 show that the crushing force can represent PSD as accurately as the breakage energy. It is also worthwhile further investigating the relationship between them. To check the correlation between the crushing force and breakage energy, the median crushing forces and breakage energies were investigated. The ratio of the median crushing forces and median breakage energies from five particle size fractions of spherical glass spheres and ceramic spheres are shown in Fig. 8. The Hertzian model incorporating size effect and no size effect (the value is constant, equals to the median breakage point of different particle diameters) were used to describe the experimental data respectively. The results show that the model that considered the size effect was more accurate than the latter model. Fig. 8 shows that the ratio of the crushing force/breakage energy decreased as the particle size increased. The correlation between the crushing force and breakage energy can be explained quantitatively from the Eqs. (4) and (9). It was found the ratio of the crushing force/breakage energy should be inversely proportional to the breakage point s_B . According to Fig. 7, the breakage point s_B is linearly dependent with the particle diameter.

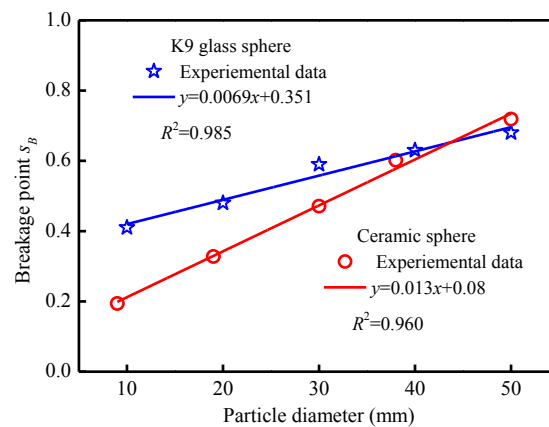


Fig. 7. The relationship between breakage point s_B and particle diameters

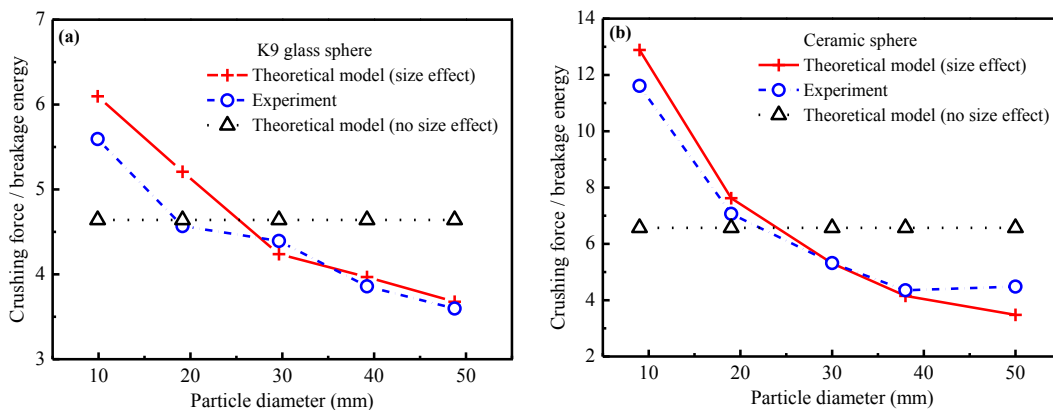


Fig. 8. The relationship between the ratio of crushing force/breakage energy and particle diameters

4.5. The transformation of distributions in terms of the crushing force and breakage energy

The breakage energy can be calculated as an integral of the contact force with respect to the displacement. Consequently, the calculation of the breakage energy requires the accurate measurement of both the force acting on the particles and deformation of the particle. It is not difficult to perform force measurement, but the measurement of deformations requires taking into account the contact deformation of the tools, particularly for small hard particles. Tavares (1998) found particle breakage energy was dependent on the ratio of particle stiffness to tool stiffness. For high stiffness, approximately 18% of the total strain energy during the stressing event is consumed by the tools, leading to the error of measurement of deformation. Based on the discussion above, the process of transformation of distributions in terms of crushing force and breakage energy has been proposed. The K9 glass sphere with a particle size of 29.64 mm was used as an example in this paper. The transformation procedure can be described as follows: (1) the median crushing force with 29.64 mm is obtained from Fig. 6 (a); (2) the median breakage energy is calculated from Fig. 8 (a); (3) the variance of crushing force and breakage energy with 29.64 mm is obtained from Fig. 6 (c); (4) the transformation of distributions in terms of crushing force and breakage energy is accomplished by Eq. (10). For example, Fig. 9 presents a breakage energy distribution of the glass spheres obtained from crushing force distribution by means of the above described transformation procedure.

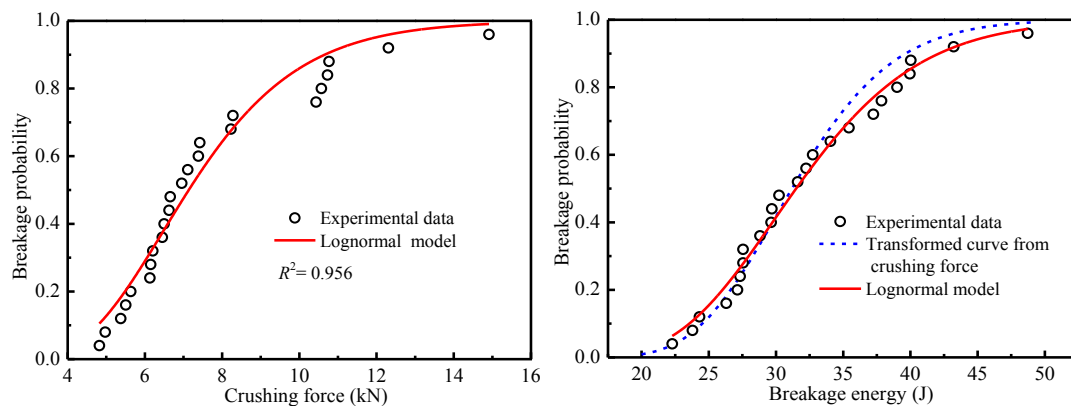


Fig. 9. The cumulative distribution functions for breakage probability of K9 glass spheres with 29.64 mm in terms of the crushing and force breakage energy

5. Conclusions

In this paper the particle strength distribution (PSD) in terms of the crushing force and breakage energy and the relationship between crushing force and breakage energy were discussed. The main findings from this study are:

- The Hertzian contact model was examined and found to be suitable to describe the contact force-displacement for the K9 glass spheres and ceramic spheres with different sizes.
- Selecting the lognormal function as a PSD representative, the parameters in the lognormal function were performed. The median crushing force and breakage energy for the K9 glass spheres and ceramic spheres were found to be linearly dependent on the square diameter of particles. The variance was found to be linearly decreased with the mean diameter of particles for K9 glass sphere. However, for ceramic sphere the variance was found to only be material dependent and was size independent.
- Previous studies (Aman et al., 2010) showed that breakage point s_B was found to be a weak function of particle size and therefore it is assumed to be a function of the material only and independent of particle size at a narrow size range. However, our study showed that the breakage point s_B was linearly dependent with the particle diameter rather than being independent of particle size for all tested materials. The relationship between the ratio of the crushing force/breakage energy was inversely proportional to the particle diameter. Based on this relationship it is possible to simply convert the crushing force to breakage energy.

Acknowledgements

The Fundamental Research Funds supported this work for the National Natural Science Foundation of China (NO. 52074308), the Central Universities (NO.2010YH11) and Shenhua Ningxia Coal Industry Group Co., Ltd. Tai xi Coal Preparation Plant, Shi Zuishan Ningxia 753000, China.

References

- WU, S.Z., CHAU, K.T., YU, T.X., 2004. *Crushing and fragmentation of brittle spheres under double impact test*. Powder Technology, 143-144, 41-55.
- NADOLSKI, S., KLEIN, B., KUMAR, A., 2014. *An energy benchmarking model for mineral comminution*. Minerals Engineering, 65, 178-186.
- MARTINS, S., 2016. *Size-energy relationship in comminution incorporating scaling laws and heat*. International Journal of Mineral Processing, 153, 29-43,
- SHI, F.N., 2016. *A review of the applications of the JK size-dependent breakage model Part 2: Assessment of material strength and energy requirement in size reduction*. International Journal of Mineral Processing, 157, 36-45,
- SHI, F.N., KOJOVIC, T., 2007. *Validation of a model for impact breakage incorporating particle size effect*. International Journal of Mineral Processing, 82, 156-163.
- TROMANS, D., 2008. *Mineral comminution: Energy efficiency considerations*, Minerals Engineering, 21, 613-620.
- FUERSTENAU, D.W., ABOUZEID, A.Z.M., 2002. *The energy efficiency of ball milling in comminution*. International Journal of Mineral Processing, 67, 161-185.
- VOGEL, L., PEUKERT, W., 2003. *Breakage behaviour of different materials-construction of a mastercurve for the breakage probability*. Powder Technology, 129, 101-110.
- ZHANG, Q.B., ZHAO, J., 2014. *A Review of Dynamic Experimental Techniques and Mechanical Behavior of Rock Materials*. Rock Mechanics & Rock Engineering, 47(4), 1411-1478.
- GONG, D.Z., NADOLSKI, S., SUN, C.B., 2018. *The effect of strain rate on particle breakage characteristics*. Powder Technology, 339, 595-605.
- TAVARES, L.M., KING, R.P., 1998. *Single-particle fracture under impact loading*. International Journal of Mineral Processing, 54, 1-28.
- LIBURKIN, R., PORTNIKOV, D., KALMAN, H., 2015. *Comparing particle breakage in an uniaxial confined compression test to single particle crush tests-model and experimental results*. Powder Technology, 284, 344-354.
- CHAU, K.T., WEI, X.X., WONG, R.H.C., 2000. *Fragmentation of brittle spheres under static and dynamic compressions: experiments and analyses*. Mechanics of materials, 32(9), 543-554.
- CHAUDHRI, M.M., 2004. *Impact breakage of semi-brittle spheres*. Powder Technology. 143, 31-40.
- HUANG, J., XU, S., YI, H., 2014. *Size effect on the compression breakage strengths of glass particles*. Powder Technology, 268, 86-94.
- PORTNIKOV, D., KALMAN, H., 2014. *Determination of elastic properties of particles using single particle compression test*, Powder Technology, 268, 244-252.
- AMAN, S., TOMAS, J., KALMAN, H., 2010. *Breakage probability of irregularly shaped particles*. Chemical Engineering Science, 65, 1503-1512.
- ROZENBLAT, Y., PORTNIKOV, D., LEVY, A., 2010. *Strength distribution of particles under compression*. Powder Technology, 208, 215-224.
- GUNDEPUDI, M.K., SANKAR, B.V., MECHOLSKY, J.J., 1997. *Stress analysis of brittle spheres under multiaxial loading*. Powder Technology, 94, 153-161.
- COUROYER, C., GHADIRI, M., BRUNARD, N., 2003. *Weibull analysis of quasi-static crushing strength of catalyst particles*. Chemical Engineering Research & Design, 81(8), 953-962.
- WONG, T.F., WONG, R.H.C, CHAU, K.T., 2005. *Microcrack statistics, Weibull distribution and micromechanical modeling of compressive failure in rock*. Mechanics of Materials, 38(7), 664-681.
- SUN, H.Q., ZENG, Y.W., YE Y., 2020. *Abnormal size effect of particle breakage probability under repeated impacts*. Powder Technology, 363, 629-641.
- TAVARES, L. M., ALMEIDA, R.F.D., 2020. *Breakage of green iron ore pellets*. Powder Technology, 366, 497-507.
- JOHNSON, K.L., 1985. *Contact Mechanics*, Cambridge University Press, Cambridge.
- TOMAS, J., 2000. *Particle adhesion fundamentals and bulk powder consolidation*, Kona Powder & Particle Journal, 18, 157-169.

- ANTONYUK, S., HEINRICH, S., TOMAS, J., 2010. *Energy absorption during compression and impact of dry elastic-plastic spherical granules*. *Granular Matter*, 12(1), 15-47.
- SUN, H.Q., ZENG, Y.W., REN, S.L., 2019. *Breakage probability of marble spheres under normal, repeated impacts*. *International Journal of Impact Engineering*, 130, 68-78.
- RUMPF, H., 1973. *Physical aspects of comminution and new formation of law of comminution*. *Power Technology*, 7, 145-159.
- HIRAMATSU, Y., OKA, Y., 1966. *Determination of the tensile strength of rock by a compression test of an irregular test piece*. *International Journal of Rock Mechanics & Mining ences & Geomechanics Abstracts*, 3(2), 89-90.